

iWalker: Imperative Visual Planning for Walking Humanoid Robot

Xiao Lin¹, Yuhao Huang², Taimeng Fu¹, Xiaobin Xiong², and Chen Wang¹

Abstract—Humanoid robots, with the potential to perform a broad range of tasks in environments designed for humans, have been deemed crucial for the basis of general AI agents. When talking about planning and controlling, although traditional models and task-specific methods have been extensively studied over the past few decades, they are inadequate for achieving the flexibility and versatility needed for general autonomy. Learning approaches, especially reinforcement learning, are powerful and popular nowadays, but they are inherently "blind" during training, relying heavily on trials in simulation without proper guidance from physical principles or underlying dynamics. In response, we propose a novel end-to-end pipeline that seamlessly integrates perception, planning, and model-based control for humanoid robot walking. We refer to our method as iWalker, which is driven by imperative learning (IL), a self-supervising neuro-symbolic learning framework. This enables the robot to learn from arbitrary unlabeled data, significantly improving its adaptability and generalization capabilities. In experiments, iWalker demonstrates effectiveness in both simulated and real-world environments, representing a significant advancement toward versatile and autonomous humanoid robots.

I. INTRODUCTION

The demand for autonomous humanoid robots has surged in recent years, as they offer unique capabilities in human-centric environments [1]. Unlike wheeled or tracked robots, humanoid robots can navigate complex spaces, climb stairs, and open doors, making them ideal for roles such as personal assistants [2] and emergency responders [3]. As urban areas grow more complex, the use of humanoid robots in these roles is expected to rise significantly [4].

Autonomous planning and control are key to realizing the full potential of humanoid robots, enabling them to move efficiently and respond to their environment without human intervention [5]. To achieve this, there is an increasing trend to develop *end-to-end systems* that seamlessly connect sensory inputs to mid-level planning and low-level control, enabling flexible and robust task execution [6]. Such systems allow robots to adapt to dynamic environments, eliminating the need for task-specific reconfiguration or reengineering.

However, traditional methods of autonomous robot control, such as those relying on pre-defined pipelines and manually tuned parameters, face significant limitations in terms of unreliability and scalability [7]–[11]. These approaches typically require the construction of 3D or 2.5D

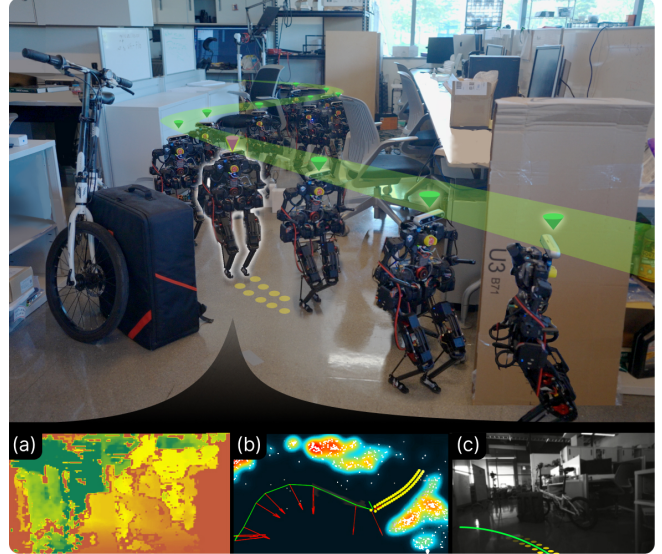


Fig. 1: A humanoid robot navigates autonomously through a messy office using iWalker. (a) is the input depth image; (b) is a visualization of the projected collision map; and (c) is a visualization of the planned path and footsteps.

maps, either through pre-measurement or online computation [12], which needs very careful configurations. Consequently, applying these methods to a wide variety of tasks remains challenging, as extensive re-engineering is often necessary when transitioning across different environments.

Learning-based approaches such as reinforcement learning and imitation learning, offer promising alternatives for planning and locomotion [13], [14]. However, these methods often suffer from training inefficiency, such as relying on stochastic sampling across vast action spaces or requiring extensive expert demonstrations [15]. This limits their ability to generalize effectively in real-world applications. Reinforcement learning methods often face challenges in generating precise low-level actions when given high-dimensional image inputs [16]. Additionally, approaches of optimizing perception, planning, and control modules separately can easily lead to suboptimal performance [17], [18].

To overcome these challenges, we introduce a novel vision-to-control pipeline based on imperative learning (IL) [19]–[23] to realize sense-plan-act pipeline for humanoid navigation in an end-to-end manner. Our proposed system, iWalker, represents a framework that connects visual inputs directly to footstep control, bypassing the need for map construction and manual tuning. By integrating a collision map and model predictive control (MPC) loss derived from

¹The Spatial AI & Robotics (SAIR) Lab, Computer Science and Engineering, University at Buffalo, NY 14260, USA. Email: {xiaol, taimengf, chenw}@sairlab.org

²The Wisconsin Expeditious Legged Locomotion (WELL) Lab, Mechanical Engineering, University of Wisconsin-Madison, WI 53706, USA. Email: {yuhao.huang, xiaobin.xiong}@wisc.edu

[†]The project page and a real-time video demonstration for iWalker are available at <https://sairlab.org/iwalker/>.

any unlabeled depth data, iWalker leverages gradient-based optimization with embedded physics information, significantly enhancing its flexibility and generalization capabilities. This approach simplifies traditional pipelines while offering improved performance, marking a significant step forward for walking autonomous humanoid robots.

In summary, the main contributions of this paper are:

- We designed a self-supervised training pipeline for humanoid robot walking systems, which can infuse physical constraints into planning networks via MPC-based IL. This results in a higher training efficiency and generalization ability than prior methods.
- We proposed an end-to-end hierarchical inference pipeline for humanoid sense-plan-act walking, which largely reduces the system’s complexity and eliminates compounded errors that exist in modular systems. eriments, we demonstrated that iWalker can easily adapt to various indoor environments, showing consistent performance of dynamical feasibility in both simulations and on the real robot.

II. RELATED WORK

A. Path Planners

Classic path planning methods have demonstrated significant success in navigating complex terrains. For example, Cao et al. [24], Wellhausen and Hutter [11], and Yang et al. [25] combined terrain analysis, mapping, and motion-primitive searches in real-world applications, including the DARPA SubT Challenge [17]. These methods employ path search techniques such as lazyPRM [26] and PRM* [27], which have proven effective in various settings. Recent advances shifted toward end-to-end planners that directly map sensory inputs to paths [28] or control actions [29], addressing issues like increased latency and reduced robustness commonly found in modular systems. These planners often rely on imitation of expert demonstrations [30] or simulation-based training [31]. Reinforcement learning (RL) provides an alternative by enabling policies to explore the action space independently of expert labels. While RL benefits from exploration, it also encounters obstacles such as the sim-to-real gap and low sample efficiency [32]. Techniques like auxiliary tasks [33] have been proposed to address these limitations, while being sensitive to the accuracy of the data.

B. Humanoid Robot Walking Planners

Humanoid robots often require mid-level step planners to convert rough path plans into executable step sequences. Hildebrandt et al. [34] combined mobile platform planners with step planners to enhance real-time planning, using sensor-based navigation to generate paths in dynamic environments. Xiong et al. [35] developed a step-to-step MPC based on a hybrid-linear inverted pendulum (H-LIP) model, optimizing footsteps while using feedback control to handle model approximation errors. Control methods based on the divergent component of motion (DCM) [7] allow continuous

adjustments of current stepping through closed-loop control. However, traditional methods typically separate high-level path planning from mid-level step planning and low-level control. Our work addresses this gap by integrating end-to-end planning and control from visual sensor inputs, employing task-level losses and combining collision maps with MPCs for physics-based guidance, improving general performance and adaptability across diverse environments.

C. Imperative Learning

Imperative learning (IL) is an emerging neural-symbolic learning framework based on bi-level optimization (BLO) [19]. It has been applied to various fields in robotics [20]–[23], [36] due to its enhanced accuracy offered by the symbolic reasoning engines and self-supervised learning nature. For instance, iSLAM [20] formulated the simultaneous localization and mapping (SLAM) problem as a BLO, enabling the reciprocal optimization of front-end visual odometry and back-end pose graph optimization. iMatching [22] showcased a feature-matching model trained through self-supervision by performing bundle adjustment without requiring labeled data. iA* [23] co-optimizes a neural network and the A* algorithm for global path planning, achieving enhanced performance and efficiency by using the network to predict a constrained search space for the A* algorithm. iMTSP [21] tackled the min-max multiple traveling salesman problem (MTSP), utilizing a task assignment network at the upper level and a standard TSP solver at the lower level of the BLO process. iPlanner [36] employed a planning network to generate waypoints, followed by a closed-form solution for path interpolation in lower-level optimization.

Different from prior works, our iWalker incorporates robot dynamics models into an end-to-end and hierarchical learning pipeline, predicting physically feasible solutions. To the best of our knowledge, our iWalker is one of the first end-to-end learned vision-to-control solutions for humanoid robots walking, enabling a perception-plan-act pipeline.

III. METHODOLOGY

As shown in Fig. 2, iWalker serves as an end-to-end visual mid-level stepping controller, which connects sensors and commands to low-level control for a humanoid robot.

A. Overall Structure of iWalker

As illustrated in Fig. 3, iWalker is a hierarchical system consisting of two primary components, a visual path planner and a mid-level step controller, each accompanied by a bi-level optimization (BLO). The visual path planner, implemented as a neural network, processes depth images and goal positions to generate sequences of waypoints. Building on this, the step controller, another simple network, receives the path and the robot’s state as inputs and outputs the next feasible footstep for low-level whole-body control.

This design offers several advantages for walking a humanoid robot. First, the system implements a complete sense-plan-act pipeline, eliminating the necessity for complex online map construction. Second, leveraging imperative



Fig. 2: The system pipeline of our humanoid robot, where iWalker is a walking planner for mid-level footstep control.

learning [19], the system can be trained in a self-supervised end-to-end manner, which mitigates the compounding errors introduced by individual components. Third, during training, constraints from the robot’s dynamic models are infused into the networks by solving bi-level optimizations, ensuring that the planned paths and footsteps are physically feasible for our chosen humanoid robot. Since both the visual planner and the step controller are based on imperative learning (IL), we refer to them as “iPath” and “iStepper”, respectively. We next introduce the details of the two modules in Section III-B and Section III-C, respectively. The methods of low-level whole-body control are presented in Section III-D.

B. Dynamics-aware Path Planning (iPath)

As a visual path planner, iPath takes a goal location and a depth image to generate paths, which guide the robot toward the target while avoiding obstacles. To infuse dynamics, we follow the imperative learning (IL) framework [19] with physics-constrained MPCs to train iPath via a bi-level optimization (BLO). Specifically, our goal is to train a network f_{path} so that it outputs a trajectory that can be easily tracked and fitted by our chosen MPC, resulting in a minimum upper-level loss U_{path} subjecting to a lower-level loss L_{path} . The optimization schemes can be formulated as:

$$\min_{w_p} U_{\text{path}}(f_{\text{path}}(d, g; w_p), \phi^*), \quad (1)$$

$$\text{s.t. } \phi^* = \arg \min_{\phi} L_{\text{path}}(\hat{\phi}, \phi), \quad (2)$$

$$\hat{\phi} = f_{\text{path}}(d, g; w_p), \quad (3)$$

$$U_{\text{path}} = \text{MSE}(\hat{\phi}, \phi^*), \quad (4)$$

where $\hat{\phi}$ is the predicted trajectory from network f_{path} with w_p as weights, d as depth inputs, and g as the goal location. Specifically, the self-supervision of the upper-level network training (1) is achieved by enforcing the lower-level optimization in (2), which is an MPC requiring no labels. The objective L_{path} of the lower-level MPC for N states is:

$$L_{\text{path}}(\hat{\phi}, \phi) = \sum_k^N (\phi_k - \hat{\phi}_k)^T Q (\phi_k - \hat{\phi}_k) + u_k^T R u_k, \quad (5)$$

$$\text{s.t. } \phi_{k+1} = \xi(\phi_k, u_k), \quad (6)$$

where k is time index; the predicted trajectory $\hat{\phi}$ is used as reference for state ϕ ; u is dynamic inputs; ξ is the MPC transition function; and Q and R are weight matrices of quadratic costs. Intuitively, if U_{path} and L_{path} reach their minimum, which means the network’s prediction is nearly

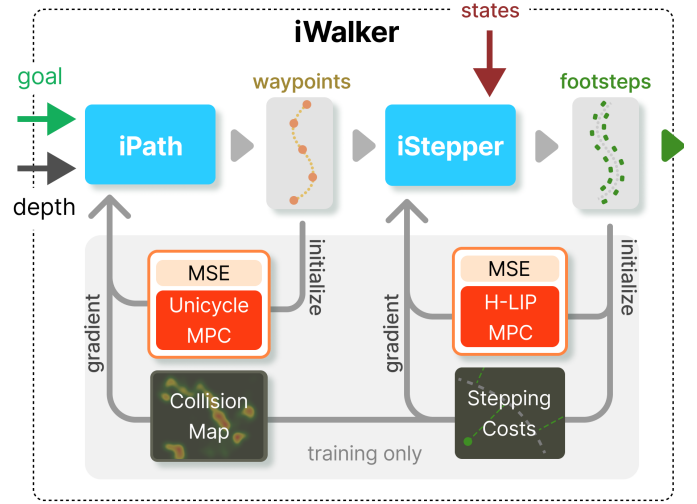


Fig. 3: iWalker includes two bi-level optimizations (BLO) based on imperative learning (IL). The first BLO optimizes iPath to predict a dynamically optimal and collision-safe path, while the second BLO optimizes iStepper to predict physically feasible footsteps for low-level controllers.

optimized, we can say prediction $\hat{\phi}$ is physically feasible.

To optimize a smoother trajectory ϕ^* , we choose a unicycle MPC which minimizes the lower-level loss L_{path} . By penalizing linear acceleration and angular velocity, we can improve the smoothness and evenness of the trajectory ϕ . This is because a constant speed ensures evenly distributed waypoints and a low angular velocity minimizes turnings. The discrete dynamics of the unicycle model is given by:

$$x_{k+1} = x_k + v_k \cos \theta_k \cdot dt, \quad (7a)$$

$$y_{k+1} = y_k + v_k \sin \theta_k \cdot dt, \quad (7b)$$

$$v_{k+1} = v_k + a_k \cdot dt, \quad (7c)$$

$$\theta_{k+1} = \theta_k + \omega_k \cdot dt, \quad (7d)$$

where we use $[x_k, y_k, v_k, \theta_k]^T$ as the state vector, representing the robot’s position x_k, y_k , velocity v_k , and orientation θ_k ; $[\omega_k, a_k]^T$ is the control input, consisting of angular velocity ω_k and the acceleration a_k . To solve this non-linear unicycle dynamics we use an iterative QP solver like iLQR [37] implemented by OSQP [38], and PyPose [39] modules are used to realize BLO. A low U_{path} indicates that the predicted $\hat{\phi}$ is close to the optimized ϕ^* , and a low L_{path} means it is easy for MPC to track $\hat{\phi}$ given costs and constraints.

Although iPath shares the same network architecture with iPlanner [36], our training approach is significantly different. iPlanner only relies on multiple heuristic losses like motion cost and goal cost based on waypoint locations without any dynamics constraints, while iPath, instead, uses one single unicycle MPC loss and demonstrates superior performance enhancement across all metrics, as showed in experiments.

C. Dynamics-aware Mid-level Step Control (iStepper)

After obtaining a raw path, we need to predict a series of footsteps considering the robot’s state and dynamics.

Algorithm 1: Optimization Iteration

Input: depth d , goal g , state ε

$\hat{\phi} \leftarrow f_{\text{path}}(d, g)$

$\phi^* \leftarrow g_{\text{uni-MPC}}(\hat{\phi})$

$U_{\text{path}} \leftarrow \text{MSE}(\hat{\phi}, \phi^*)$

backward U_{path}

Initialize collision map $M_{\text{col}} \in \mathbb{Z}^{h \times w}$

$P \leftarrow \text{project}(d)$

foreach $p \in 3D \text{ point cloud } P$ **do**

$(n, m) \leftarrow \text{index}(p_x, p_y)$

$M[n, m] \leftarrow M[n, m] + 1$

$M_{\text{ESDF}} \leftarrow G(M_{\text{col}})$

$\hat{S} \leftarrow f_{\text{step}}(\hat{\phi}, \varepsilon)$

$S^* \leftarrow g_{\text{LIP-MPC}}(\hat{S}, \varepsilon)$

$U_{\text{ESDF}} \leftarrow 0$

foreach $\hat{s} \in \text{step sequence } \hat{S}$ **do**

$U_{\text{ESDF}} \leftarrow U_{\text{ESDF}} + \text{sample}(M_{\text{ESDF}}, \hat{s}_x, \hat{s}_y)$

$U_{\text{step}} \leftarrow \text{MSE}(S, S^*) + U_w(S, \bar{w}) + U_l(S, \bar{l}) + U_{\text{ESDF}}$

backward U_{step}

Optimize $f_{\text{path}}, f_{\text{step}}$

return

Similarly, we employ a second IL learning strategy for stepping predictor f_{step} , which can be formulated as:

$$\min_{w_s} U_{\text{step}}(f_{\text{step}}(\hat{\phi}, \varepsilon; w_s), S^*), \quad (8)$$

$$\text{s.t. } S^* = \arg \min_S L_{\text{step}}(\hat{S}, S), \quad (9)$$

$$\hat{S} = f_{\text{step}}(\hat{\phi}, \varepsilon; w_s), \quad (10)$$

where the network f_{step} predicts a step sequence \hat{S} given the previously predicted path $\hat{\phi}$ and current robot states ε .

To make our prediction physically feasible for step control, we employ a step-to-step (S2S) dynamics-based MPC [35]. Due to the difficulty of directly obtaining the analytical form of robot S2S dynamics, we use a linear approximation called the hybrid-linear inverted pendulum (H-LIP) model [40] to approximate robot S2S dynamics, tracking the predicted footsteps. Specifically, the H-LIP dynamics is defined as:

$$\mathbf{x}_{k+1}^{\text{H-LIP}} = A_s \mathbf{x}_k^{\text{H-LIP}} + B_s u_k^{\text{H-LIP}}, \quad (11)$$

where $\mathbf{x}_k^{\text{H-LIP}} = [\mu_k, p_k, v_k]^T$ denotes the k -th pre-impact state of the H-LIP, with μ_k , p_k , and v_k being the global center of mass (COM) position, stance foot position w.r.t COM, and velocity, respectively; u_k denotes the k -th global step size. The formulation of A_s and B_s can be found in [35].

Since the 2D H-LIP is based on two stacked 1D H-LIPs, modeling XY planes independently, it does not describe the robot's orientation, which essentially determines the kinematic feasibility of realizable step sizes. To encode the desired step width and step length in robot's frame to the step planner, we define two extra upper-level loss functions, U_w on step width and U_l on step length, with global-to-local mapping. These additional upper-level costs are measured in the robot's local frame given path $\hat{\phi}$, with \bar{w} and \bar{l} being the

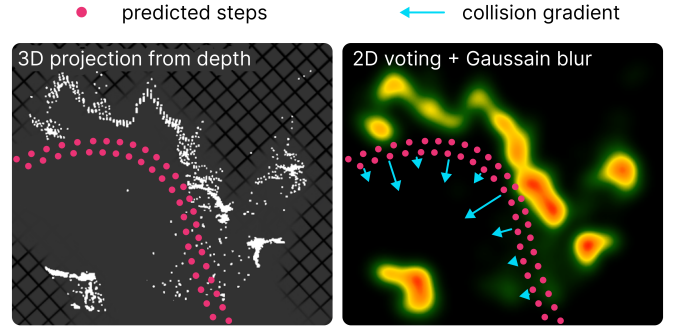


Fig. 4: A visualization of collision map and gradient. The 3D point cloud (left) is obtained from depth projection, while the right is an approximated ESDF map from blurring.

desired step width and step length, respectively:

$$U_w = \sum_k \text{MSE}(h_x(\hat{s}_k, \hat{\phi}), \bar{l}), \quad (12)$$

$$U_l = \sum_k \text{MSE}(h_y(\hat{s}_k, \hat{\phi}), \bar{w} \cdot \alpha_k), \quad (13)$$

$$\alpha_k = \begin{cases} 1, & \text{if } (k+o) \text{ is even,} \\ -1, & \text{if } (k+o) \text{ is odd,} \end{cases} \quad (14)$$

where h_x and h_y are functions that map one step location s_k to its width and length in the robot's local frame, the origin and orientation are determined by the closest point on the path $\hat{\phi}$ from \hat{s}_k ; To distinguish left-right stepping, o is 0 if the robot is currently standing with the left leg, otherwise 1.

To enable obstacle avoidance capability, we build a Euclidean Signed Distance Field (ESDF) map M_{ESDF} as described in the second block of Algorithms 1 and visualized in Fig. 4. The ESDF map is used to calculate the collision costs and gradients subject to step locations, which is the key to ensuring collision-free stepping. Additionally, we apply a Gaussian blurring G on the collision map to filter noise and ensure a continuous gradient space, guiding the footsteps to safer regions. We sample the collision costs by the stepping locations to ensure the feasibility of actual footsteps, instead of measuring directly from the raw waypoints.

The complete upper-level loss U_{step} for step planning combining losses mentioned above is defined as:

$$U_{\text{step}} = \text{MSE}(\hat{S}, S^*) + U_w + U_l + U_{\text{ESDF}}. \quad (15)$$

This loss enforces the physical constraints described by the H-LIP, step targets, and collision costs. The corresponding part can be found in the second and third blocks in Algorithm 1. For notation simplicity, we omitted the cost weights that balance multiple losses. It is necessary to note that back-propagating the step planning loss U_{step} produces gradients for both path planner f_{path} and step controller f_{step} , which is the key to eliminate accumulated errors between modules by end-to-end learning. In contrast, path planning loss U_{path} will only backward gradients for the weights in f_{path} . A detailed pseudo-code for one iteration of bi-level optimization based on imperative learning is listed in Algorithm 1.

D. Whole Body Control

Once the desired footstep is determined, the next step is to execute it by a task-space whole-body controller [41]. We formulate the controller in (16), where the tasks include tracking the swing foot trajectory, swing foot orientation, torso orientation, centroidal momentum, and contact forces.

$$\min_{\dot{q}, \tau, F_j} \sum_{i=1}^{N_t} \|J_i \dot{q} + \dot{J}_i \dot{q} - \dot{x}_i^{\text{des}}\|_{W_i}^2 + \sum_{j=1}^{N_c} \|F_j\|_{W_f}^2 + \|\ddot{q}\|_{W_{\ddot{q}}}^2, \quad (16a)$$

$$\text{s.t.} \quad H_b \ddot{q} + h_b(q, \dot{q}) = B\tau + \sum_{j=1}^{N_c} J_j^\top F_j, \quad (16b)$$

$$A(F_j) \leq 0, \quad \forall j = 1, \dots, N_c, \quad (16c)$$

where q denotes the robot configuration, W denotes the weights on the cost, J_i is the Jacobian of i -th task, J_j is the j -th contact Jacobian, N_t is the number of tasks, F_j is the contact reaction force at the foot-ground contact indexed by j , N_c is the number of contact points, $A(F_j) \leq 0$ denotes the linearized contact force constraints, H_b is the mass matrix, h_b denotes the Coriolis and gravity vector, τ is the motor torques to solve for execution, and B is constant matrix mapping the motor torques to generalized forces on the robot joints. As we can see, the i -th task space goal is set as a cost in the quadratic program with priority implicitly being enforced with weight W_i . Additionally, regularization costs are added to the decision variables \ddot{q} and F_j with small weights $W_{\ddot{q}}$ and W_f , respectively. To effectively follow our first planned step location s_0 from iWalker, a reference polynomial trajectory is fitted according to the current swinging foot’s state.

IV. EXPERIMENTS

A. Implementation, Platform, and Baselines

We deploy our algorithms on BRUCE [41], a 0.6 m tall humanoid robot, featuring five degrees of freedom (DoF) per leg, proprioceptive actuators, tactile foot switches. Additionally, we leverage an IMU for body sensing and a RealSense D455 camera mounted on top for depth perception. The system runs on multiple processes. The main Python process oversees overall system inputs and outputs, while individual modules like state estimation (using a modified Kalman filter [41]), mid-level control, low-level control, visual odometry [42], and our iWalker operate as separate processes. All processes are run on a laptop-level computing platform, which is equipped with a 6900HS AMD CPU and a 3070Ti GPU, running Ubuntu 20.04 and ROS1 [43].

Since iWalker is one of the first vision-to-control learning-based solutions for humanoid robots, we have very few open-sourced baseline solutions to compare. As a result, we will mainly compare with iPlanner, as iPlanner and iPath share the same network structure. Given that iPlanner only predicts paths, we attach our trained iStepper to it for a comprehensive comparison, which can also demonstrate the adaptability of our proposed iStepper. We refer to fine-tuned “iPlanner” in our training environments as “iPlanner*”.

TABLE I: The violation of dynamical feasibility (\downarrow).

Method	Stair	Office	Corridor	Corner
iPlanner + iStepper	1.4840	2.4366	1.286	0.8140
iPlanner* + iStepper	3.5751	2.2521	5.2924	5.7913
iWalker	1.4321	0.4827	0.4677	0.5330

TABLE II: The evaluation of collision safety (\downarrow).

Method	Stair	Office	Corridor	Corner
iPlanner + iStepper	11.969	21.522	4.4698	5.8537
iPlanner* + iStepper	12.425	24.905	3.8941	6.5459
iWalker	10.167	8.9221	3.1317	3.998

TABLE III: The performance of waypoint stability (\downarrow).

Method	Stair	Office	Corridor	Corner
iPlanner + iStepper	89.8	3.20	19.1	1.00
iPlanner* + iStepper	71.6	24.6	33.3	38.3
iWalker	31.0	0.90	3.32	0.71

B. Quantitative Comparison

We collected 1185 frames from 12 different indoor scenes in real-world environments using a RealSense camera. Among them, 8 scenes are for training and the other 4 scenes (stairs, offices, corridors, and corners) are for testing.

1) *The Dynamical Feasibility*: To measure the dynamical feasibility of predicted steps, we measure the low-level costs from unicycle and H-LIP MPC. Intuitively, lower MPC costs indicate less violation of the robot’s dynamics and easier actuation. As shown in Table I, iWalker, trained iPath and iStepper in a hierarchical end-to-end manner, eliminates the compound errors and achieves significant improvement in dynamical feasibility, while both iPlanner and iPlanner* are unaware of dynamics needed for low-level control.

2) *Collision Safety*: To assess collision safety, we calculate the collision risk by sampling the collision ESDF maps at the predicted footstep locations. Intuitively, lower risk values correspond to safer prediction, indicating improved obstacle avoidance along the step sequence. As shown in II, iWalker has the lowest collision risk for the predicted steps, while both iPlanner and iPlanner only penalize collision costs at waypoints, leaving footstep-level safety unaddressed.

3) *Waypoints Stability*: To measure the stability of predicted waypoints before step control, we measure the variance of the waypoint interval as an indicator of waypoint evenness. This is because evenly distributed waypoints can lead to easier MPC optimization and smoother low-level actuation. As shown in Table III, iPlanner, which was trained on accurate LiDAR maps, fails to generate stable waypoints given our noisy depth sensing, no matter whether fine-tuned or not. In contrast, iWalker consistently improves waypoint evenness by incorporating dynamic information.

C. Real-time Demo in Simulation

We primarily tested our complete sense-plan-act pipeline for the humanoid robot BRUCE with iWalker within the

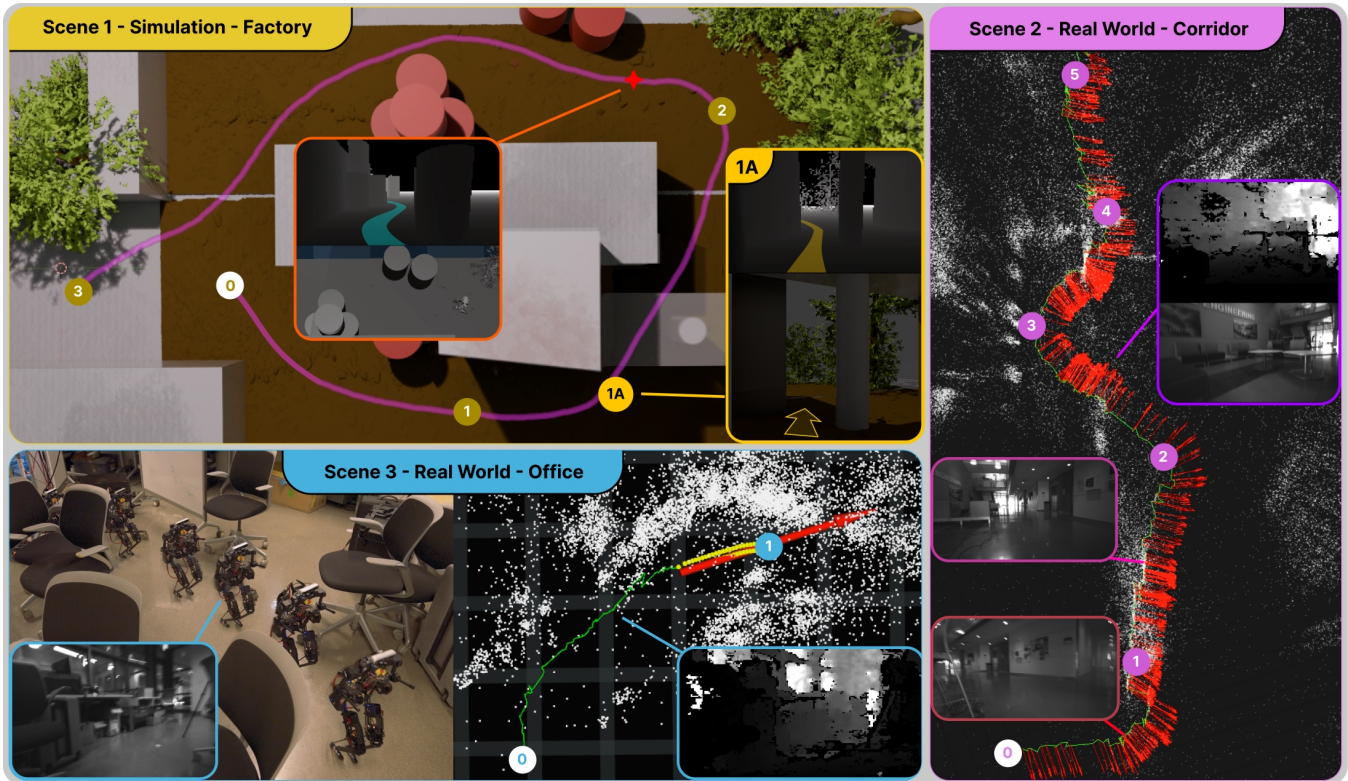


Fig. 5: We presents both simulation and real-world demonstrations of our robot’s navigation capabilities across distinct environments. Goal points are explicitly labeled. In **Scene 1**, the robot with iWalker trained on real-world data navigates in a factory-like scene using only three goal points, showcasing efficient navigation in unseen environments. In **Scene 2**, the robot traverses a 10-meter corridor with many turns, showing its proficiency in handling long pathways. In **Scene 3**, iWalker navigates a short path through environments with irregular shapes, illustrating its adaptability to noisy depth.

MuJoCo simulation environment [44]. It is worth noting that in this experiment, iWalker is only trained with real-world noisy depth images, without seeing any images from simulation. In Fig. 5-Scene 1, the robot smoothly navigates through a huge factory-like environment. This demonstrates that iWalker can effectively adapt to unseen simulated environments largely different from real-world training data. Impressively, iWalker is able to complete fully autonomous navigation across half of the map from point 2 to point 3 under one single goal command, traversing through barrels and unseen obstacles. Moreover, iWalker is able to navigate through a narrow gap between the wall and the pillar without collision as highlighted in Fig. 5-1A. With stable low-level control and precise state estimation in the simulation, iWalker can always plan and walk smoothly even in unseen scenes.

D. Real-time Demo with Real Humanoid Robot

We next evaluate iWalker’s performance on the real robot. We first command the robot to navigate through a long path in Fig. 5-Scene 2, where the robot traversed a long 10-meter corridor with multiple turns. This verifies the effectiveness of iWalker in large-scale environments. In addition, we tested iWalker’s ability to pass through messy environments like Fig. 5-Scene 3, where iWalker successfully navigates through a narrow path in a cluttered office scene where chairs are

placed randomly. These tests demonstrate iWalker’s generalization ability and consistent performance in unseen, structured simulation scenes as well as noisy real-world settings, validating its effectiveness across a variety of scenes. A video of the real-time demonstration for iWalker is available at the project page <https://sairlab.org/iwalker/>, in which we test under more settings and environments.

V. CONCLUSION & LIMITATIONS

We introduced iWalker, a vision-to-control pipeline developed for humanoid robot walking. By incorporating two MPC-based bilevel optimizations through imperative learning, iWalker enables efficient and robust self-supervised training on visual input data, predicting dynamically optimal, collision-free paths and physically feasible footsteps for low-level actuation. Our experiments, conducted in simulation and on real robots, demonstrate the capability of iWalker to navigate through various simulated scenes and unseen real-world environments. However, the system still faces several limitations. The instability of low-level controllers and the limited scale of our platform restrict testing on more challenging terrains, limiting the comprehensiveness of our evaluations. Addressing these issues is critical for bringing our method to more challenging environments.

REFERENCES

- [1] Y. Tong, H. Liu, and Z. Zhang, "Advancements in humanoid robots: A comprehensive review and future prospects," *IEEE/CAA Journal of Automatica Sinica*, vol. 11, no. 2, pp. 301–328, 2024.
- [2] J. Mišeikis, P. Caroni, P. Duchamp, A. Gasser, R. Marko, N. Mišeikienė, F. Zwilling, C. De Castelbajac, L. Eicher, M. Früh, et al., "Lio-a personal robot assistant for human-robot interaction and care applications," *IEEE Robotics and Automation Letters*, vol. 5, no. 4, pp. 5339–5346, 2020.
- [3] H. Chitkena, F. Sanfilippo, and S. Ma, "Robotics in search and rescue (sar) operations: An ethical and design perspective framework for response phase," *Applied Sciences*, vol. 13, no. 3, p. 1800, 2023.
- [4] I. Tiddi, E. Bastianelli, E. Daga, M. d'Aquin, and E. Motta, "Robot-city interaction: Mapping the research landscape—a survey of the interactions between robots and modern cities," *International Journal of Social Robotics*, vol. 12, pp. 299–324, 2020.
- [5] J. Ahn, S. J. Jorgensen, S. H. Bang, and L. Sentis, "Versatile locomotion planning and control for humanoid robots," *Frontiers in Robotics and AI*, vol. 8, p. 712239, 2021.
- [6] O. Doukhi and D.-J. Lee, "Deep reinforcement learning for end-to-end local motion planning of autonomous aerial robots in unknown outdoor environments: Real-time flight experiments," *Sensors*, vol. 21, no. 7, p. 2534, 2021.
- [7] M. Khadiv, A. Herzog, S. A. A. Moosavian, and L. Righetti, "Walking control based on step timing adaptation," *IEEE Transactions on Robotics*, vol. 36, no. 3, pp. 629–643, 2020.
- [8] Z. Gao, X. Chen, Z. Yu, M. Zhu, R. Zhang, Z. Fu, C. Li, Q. Li, L. Han, and Q. Huang, "Autonomous navigation with human observation for a biped robot," in *2021 IEEE International Conference on Unmanned Systems (ICUS)*. IEEE, 2021, pp. 780–785.
- [9] J. Delfin, H. M. Becerra, and G. Archavaleta, "Humanoid navigation using a visual memory with obstacle avoidance," *Robotics and autonomous systems*, vol. 109, pp. 109–124, 2018.
- [10] D. Maier, C. Lutz, and M. Benezewitz, "Integrated perception, mapping, and footstep planning for humanoid navigation among 3d obstacles," in *2013 IEEE/RSJ international conference on intelligent robots and systems*. IEEE, 2013, pp. 2658–2664.
- [11] L. Wellhausen and M. Hutter, "Rough terrain navigation for legged robots using reachability planning and template learning," in *2021 IEEE/RSJ International Conference on Intelligent Robots and Systems (IROS)*. IEEE, 2021, pp. 6914–6921.
- [12] Z. Li, J. Zeng, S. Chen, and K. Sreenath, "Autonomous navigation of underactuated bipedal robots in height-constrained environments," *The International Journal of Robotics Research*, vol. 42, no. 8, pp. 565–585, 2023.
- [13] Z. Li, X. Cheng, X. B. Peng, P. Abbeel, S. Levine, G. Berseth, and K. Sreenath, "Reinforcement learning for robust parameterized locomotion control of bipedal robots," in *2021 IEEE International Conference on Robotics and Automation (ICRA)*. IEEE, 2021, pp. 2811–2817.
- [14] Z. Li, X. B. Peng, P. Abbeel, S. Levine, G. Berseth, and K. Sreenath, "Reinforcement learning for versatile, dynamic, and robust bipedal locomotion control," 2024. [Online]. Available: <https://arxiv.org/abs/2401.16889>
- [15] M. Bojarski, "End to end learning for self-driving cars," *arXiv preprint arXiv:1604.07316*, 2016.
- [16] A. Allshire, R. Martín-Martín, C. Lin, S. Manuel, S. Savarese, and A. Garg, "Laser: Learning a latent action space for efficient reinforcement learning," in *2021 IEEE International Conference on Robotics and Automation (ICRA)*. IEEE, 2021, pp. 6650–6656.
- [17] C. Cao, L. Nogueira, H. Zhu, J. Keller, G. Best, R. Garg, D. Kohanbash, J. Maier, S. Zhao, F. Yang, et al., "Exploring the most sectors at the darpa subterranean challenge finals," *Field Robotics*, 2023.
- [18] S. Levine, C. Finn, T. Darrell, and P. Abbeel, "End-to-end training of deep visuomotor policies," *Journal of Machine Learning Research*, vol. 17, no. 39, pp. 1–40, 2016.
- [19] C. Wang, K. Ji, J. Geng, Z. Ren, T. Fu, F. Yang, Y. Guo, H. He, X. Chen, Z. Zhan, Q. Du, S. Su, B. Li, Y. Qiu, Y. Du, Q. Li, Y. Yang, X. Lin, and Z. Zhao, "Imperative learning: A self-supervised neural-symbolic learning framework for robot autonomy," *arXiv preprint arXiv:2406.16087*, 2024. [Online]. Available: <https://arxiv.org/abs/2406.16087>
- [20] T. Fu, S. Su, Y. Lu, and C. Wang, "iSLAM: Imperative SLAM," *IEEE Robotics and Automation Letters (RA-L)*, 2024. [Online]. Available: <https://arxiv.org/abs/2306.07894>
- [21] Y. Guo, Z. Ren, and C. Wang, "iMTSP: Solving min-max multiple traveling salesman problem with imperative learning," in *IEEE/RSJ International Conference on Intelligent Robots and Systems (IROS)*, 2024. [Online]. Available: <https://arxiv.org/abs/2405.00285>
- [22] Z. Zhan, D. Gao, Y.-J. Lin, Y. Xia, and C. Wang, "iMatching: Imperative correspondence learning," in *European Conference on Computer Vision (ECCV)*, 2024. [Online]. Available: <https://arxiv.org/abs/2312.02141>
- [23] X. Chen, F. Yang, and C. Wang, "iA*: Imperative learning-based a* search for pathfinding," *arXiv preprint arXiv:2403.15870*, 2024. [Online]. Available: <https://arxiv.org/abs/2403.15870>
- [24] C. Cao, H. Zhu, F. Yang, Y. Xia, H. Choset, J. Oh, and J. Zhang, "Autonomous exploration development environment and the planning algorithms," in *2022 International Conference on Robotics and Automation (ICRA)*. IEEE, 2022, pp. 8921–8928.
- [25] B. Yang, L. Wellhausen, T. Miki, M. Liu, and M. Hutter, "Real-time optimal navigation planning using learned motion costs," in *2021 IEEE International Conference on Robotics and Automation (ICRA)*. IEEE, 2021, pp. 9283–9289.
- [26] L. Kavrakci and R. Bohlin, "Path planning using lazy prm," in *International Conference on Robotics and Automation*, vol. 1. IEEE, 2000, pp. 521–528.
- [27] S. Karaman and E. Frazzoli, "Sampling-based algorithms for optimal motion planning," *The International Journal of Robotics Research*, vol. 30, no. 7, pp. 846–894, 2011.
- [28] Y. Kim, C. Kim, and J. Hwangbo, "Learning forward dynamics model and informed trajectory sampler for safe quadruped navigation," *arXiv preprint arXiv:2204.08647*, 2022.
- [29] A. Sadat, S. Casas, M. Ren, X. Wu, P. Dhawan, and R. Urtasun, "Perceive, predict, and plan: Safe motion planning through interpretable semantic representations," in *European Conference on Computer Vision*. Springer, 2020, pp. 414–430.
- [30] M. Pfeiffer, M. Schaeuble, J. Nieto, R. Siegwart, and C. Cadena, "From perception to decision: A data-driven approach to end-to-end motion planning for autonomous ground robots," in *IEEE International Conference on Robotics and Automation (ICRA)*. IEEE, 2017, pp. 1527–1533.
- [31] A. Loquercio, E. Kaufmann, R. Ranftl, M. Müller, V. Koltun, and D. Scaramuzza, "Learning high-speed flight in the wild," *Science Robotics*, vol. 6, no. 59, p. eabg5810, 2021.
- [32] J. Ye, D. Batra, A. Das, and E. Wijmans, "Auxiliary tasks and exploration enable objectgoal navigation," in *Proceedings of the IEEE/CVF International Conference on Computer Vision*, 2021, pp. 16 117–16 126.
- [33] F. Zhu, Y. Zhu, X. Chang, and X. Liang, "Vision-language navigation with self-supervised auxiliary reasoning tasks," in *Proceedings of the IEEE/CVF Conference on Computer Vision and Pattern Recognition*, 2020, pp. 10 012–10 022.
- [34] A.-C. Hildebrandt, M. Klischat, D. Wahrmann, R. Wittmann, F. Sygulla, P. Seiwald, D. Rixen, and T. Buschmann, "Real-time path planning in unknown environments for bipedal robots," *IEEE Robotics and Automation Letters*, vol. 2, no. 4, pp. 1856–1863, 2017.
- [35] X. Xiong, J. Reher, and A. D. Ames, "Global position control on underactuated bipedal robots: Step-to-step dynamics approximation for step planning," in *2021 IEEE International Conference on Robotics and Automation (ICRA)*. IEEE, 2021, pp. 2825–2831.
- [36] F. Yang, C. Wang, C. Cadena, and M. Hutter, "iPlanner: Imperative path planning," in *Robotics: Science and Systems (RSS)*, 2023. [Online]. Available: <https://arxiv.org/abs/2302.11434>
- [37] W. Li and E. Todorov, "Iterative linear quadratic regulator design for nonlinear biological movement systems," in *First International Conference on Informatics in Control, Automation and Robotics*, vol. 2. SciTePress, 2004, pp. 222–229.
- [38] B. Stellato, G. Banjac, P. Goulart, A. Bemporad, and S. Boyd, "OSQP: an operator splitting solver for quadratic programs," *Mathematical Programming Computation*, vol. 12, no. 4, pp. 637–672, 2020. [Online]. Available: <https://doi.org/10.1007/s12532-020-00179-2>
- [39] C. Wang, D. Gao, K. Xu, J. Geng, Y. Hu, Y. Qiu, B. Li, F. Yang, B. Moon, A. Pandey, Aryan, J. Xu, T. Wu, H. He, D. Huang, Z. Ren, S. Zhao, T. Fu, P. Reddy, X. Lin, W. Wang, J. Shi, R. Talak, K. Cao, Y. Du, H. Wang, H. Yu, S. Wang, S. Chen, A. Kashyap, R. Bandaru, K. Dantu, J. Wu, L. Xie, L. Carlone, M. Hutter, and S. Scherer, "PyPose: A library for robot learning with physics-based optimization," in *IEEE/CVF Conference on Computer Vision and Pattern Recognition (CVPR)*, 2023. [Online]. Available: <https://arxiv.org/abs/2209.15428>

- [40] X. Xiong and A. Ames, "3-d underactuated bipedal walking via h-hip based gait synthesis and stepping stabilization," *IEEE Transactions on Robotics*, vol. 38, no. 4, pp. 2405–2425, 2022.
- [41] J. Shen, *Locomotion Analysis and Control of a Miniature Bipedal Robot*. University of California, Los Angeles, 2022.
- [42] K. Xu, Y. Hao, S. Yuan, C. Wang, and L. Xie, "AirVO: An illumination-robust point-line visual odometry," in *IEEE/RSJ International Conference on Intelligent Robots and Systems (IROS)*, 2023. [Online]. Available: <https://arxiv.org/abs/2212.07595>
- [43] M. Quigley, K. Conley, B. Gerkey, J. Faust, T. Foote, J. Leibs, R. Wheeler, A. Y. Ng, *et al.*, "Ros: an open-source robot operating system," in *ICRA workshop on open source software*, vol. 3, no. 3.2. Kobe, Japan, 2009, p. 5.
- [44] E. Todorov, T. Erez, and Y. Tassa, "Mujoco: A physics engine for model-based control," in *2012 IEEE/RSJ international conference on intelligent robots and systems*. IEEE, 2012, pp. 5026–5033.